Available online at www.sciencedirect.com
SCIENCE DIRECT
Polymer 46 (2005) 5929–5938
polymer
www.elsevier.com/locate/polymer

PVdF-HFP/P123 hybrid with mesopores: a new matrix for high-conducting, low-leakage porous polymer electrolyte

Chun-Guey Wu[a,*], Ming-I Lu[a], Huey-Jan Chuang[b]

[a]*Department of Chemistry, National Central University, Chung-Li 32054, Taiwan, ROC*
[b]*Materials & Electro-Optics Research Division, Chung-Shan Institute of Science and Technology, Lung-Tan 325, Taiwan, ROC*

Received 7 December 2004; received in revised form 22 April 2005; accepted 17 May 2005
Available online 14 June 2005

Abstract

Highly conducting porous polymer electrolytes comprised of poly(vinylidene-fluoride-*co*-hexafluoropropylene) (PVdF-HFP), polyethylene oxide-*co*-polypropylene oxide-*co*-polyethylene oxide (P123), ethylene carbonate (EC), propylene carbonate (PC), and $LiClO_4$ were fabricated. The PVdF-HFP/P123 hybrid polymer membranes were made with a phase inverse method and the electrolyte solution uptake was carried out in glove box to avoid the moisture contamination. It was found that when a small amount of polymer surfactant (P123) was blended into the PVdF-HFP, mesopores with well-defined sizes were formed. Impedance spectroscopy showed that the room temperature conductivity of (PVdF-HFP)/P123 polymer electrolytes increased as the content of P123 increased up to 4×10^{-3} S/cm. Nitrogen adsorption isotherms, electrolyte solution uptake, porosity measurements, and SEM micrographs showed that the enhanced conductivity was due to increase the pore volume, pore density, and electrolyte uptake. The highest conduction was found when the weight ratio of P123 to PVdF-HFP was 70%, when big channels were formed in the hybrid polymer membrane. Furthermore, blending P123 in PVDF-HFP reduced the pore size of polymer membrane, therefore, the solution leakage was also reduced. These polymer electrolytes were stable up to 4.5 V (vs Li/Li^+) and the performance of the model lithium ion battery made by sandwiching the polymer electrolyte between a $LiCoO_2$ anode and a MCMB cathode, showed great promise for the use of these polymer electrolytes in lithium ion batteries.

Keywords: Porous polymer; Solid electrolytes; Ionic conductivity

1. Introduction

Solid polymer electrolytes (SPEs) have received considerable attention, because of their potential applications in solid-state batteries, electrochromic devices and fundamental research of ion transport in disordered phases [1–3]. The use of polymer electrolytes make batteries safer, lighter, and more flexible in shape. Early research in polymer electrolytes emphasized dry polymer electrolytes based on polyethers, beginning with Wright's research about complexes of PEO and sodium salts [4]. Despite extensive researches on lithium polyether-based conductors, the conductivity of true solid electrolytes (with no liquid) is insufficient for practical applications at room temperature. One possible solution for enhancing the conductivity is adding liquid electrolyte to the polymer matrix (gel-type polymer electrolytes, GPE). Therefore, after 1990s, emphasis on research has turn to polymer gel electrolytes with room temperature conductivity as high as 10^{-3} S/cm, which is sufficient for practical use. Various polymers, such as poly(vinylidene fluoride-*co*-hexafluoropropylene) (PVdF-HFP) [5], poly(vinylidene fluoride) (PVdF) [6,7], poly(methyl methacrylate) (PMMA) [8–10], polyacrylonitrile (PAN) [11,12], poly(vinyl chloride) (PVC) [13], poly(ethylene oxide) (PEO) [14,15], and their blends [16,17] have been investigated. Among these polymers, mesoporous PVdF-HFP (developed by Bellcore in 1996, using a liquid extraction/activation method) has received special attention as one of the promising host polymers for polymer electrolytes because of its excellent mechanical strength and electrochemical stability. It is recognized that the PVdF polymer constitutes a two-phase separated gel composed of the swollen polymer chains and the solution

* Corresponding author. Tel.: +886 3 4227151x5903; fax: +886 3 4227664.
E-mail address: t610002@cc.ncu.edu.tw (C.-G. Wu).

0032-3861/$ - see front matter © 2005 Elsevier Ltd. All rights reserved.
doi:10.1016/j.polymer.2005.05.077

retained in the cavities of the porous polymer [18,19]. Therefore, it is expected that both the interaction between the carriers and the polymer chains in the swollen polymer and the amount of the liquid electrolyte incorporated into the polymer matrix contribute to the ionic conductivity.

Since the ionic conductivity of the polymer electrolyte increases with increasing amount of the liquid electrolyte incorporated into the polymer matrix, many researches have been focused on increasing the liquid electrolyte content in the PVdF-HFP matrix by controlling the components and morphology. For example, Kim et al. [20] used a blend of PVdF-HFP and PAN as a matrix polymer for the polymer electrolyte. They considered that PAN gave mechanical integrity and structural rigidity to the porous polymer without inorganic fillers. Oh and Kim [21] reported that blending PVdF-HFP and PMMA-VAc to form mesoporous GPE increased the transparency in the visible region and hence made the material suitable for electrochromic devices. Huang et al. [22–24] showed that the addition of SiO_2 was an effective way to generate micropores in the PVdF-HFP matrix. Furthermore, Saito et al. [25] found that several factors of the gel electrolyte, such as the porosity, pore size, crystallinity, chain structure, and the degree of polymerization of the polymer, dominated the conduction properties of the carriers.

In this paper, PVdF-HFP was blended with polyethylene oxide–propylene oxide block copolymer (P123) to form new hybrid polymer matrices. P123 is a stable, amorphous, transparent PEO based polymer [26]; therefore it will have good interactions with Li^+. Blending P123 into PVdF-HFP not only tunes the pore structure of the polymer electrolyte matrix and facilitates the transport of lithium ions, but also increases the transparence of the electrolyte film.

2. Experimental section

2.1. Materials

$LiClO_4$ was dried under reduced pressure prior to use. Ethylene carbonate (EC), propyl carbonate (PC), poly (vinylidenefluoride-*co*-hexafluoropropylene) (PVdF-HFP, M_W=40,000; VDF/HFP=78/22) and polyethylene oxide-*co*-polypropylene oxide-*co*-polyethylene oxide (P123, mole ratio of EO/PO/EO=30/70/30 M_W=5800) and solvents were obtained from commercial resources and used without further treatment.

2.2. Preparation of PVdF-HFP/P123 hybrid porous polymer membranes

The hybrid polymer membranes were prepared by phase inversion. Two grams of PVdF-HFP was dissolved in 8 ml pure *N*-methyl-2-pyrrolidone (NMP) or a mixture (volume ratio: 4.7–3.3) of a volatile solvent (acetone) and high boiling-point solvent (NMP). The proportion of the high boiling-point solvent is low enough to allow dissociation and high enough to allow phase separation during evaporation. In the PVdF-HFP solution, various amount of P123 was added under vigorous stirring at 60–70 °C for 12 h. After P123 was completely dissolved, the solution was blade coating on a Teflon plate (spread with the use of a blade) or spin-coated on a Teflon plate. The high viscosity polymer gel on the substrate was put into a stream atmosphere for 3–5 min to induce phase inversion. When the surface of the polymer gel was dry, it was dipped in water at room temperature for an hour to completely remove the residual NMP. After exchange of NMP with water, the film contains a substantial amount of water. The resulting film was heated in a vacuum oven at 80 °C, 10^{-1} Torr for 24 h to remove the water. After the water was evaporated, the mechanically stable free standing porous polymer membranes (200–400 μm thickness) could be peeled off from the Teflon plate. The porous polymer membranes were stored in a dry-box right after removal from the vacuum oven to avoid the absorption of moisture. The codes for the porous blend polymer films are presented as PVdF-HFP/A%P123; where A is the weight percentage of P123 with respect to the polymer blend.

2.3. The porosity of the polymer membranes

The porosity of the polymer membranes was measured by immersing the membrane into *n*-butanol for 1 h and weighing the membrane before and after absorption of the *n*-butanol. The porosity was calculated using the following equation:

$$P\% = \frac{M_b/\rho_b}{(M_p/\rho_P) + (M_b/\rho_b)}$$

where $P\%$ is porosity of the membrane, M_p the mass of membrane, M_b the mass of absorbed *n*-butanol, ρ_P the density of the membrane and ρ_b the density of *n*-butanol.

2.4. Electrolyte solution uptake and leakage of porous polymer electrolyte

In the glove box, the porous polymer membrane was cut into a disk with a diameter of 1 cm. After the thickness and mass (W_0) of the membrane disk was measured, it was soaked in a 1.0 M $LiClO_4$-EC/PC (1:1) solution at room temperature for 2 h to activate the porous polymer electrolyte. After the excrescent solution at the surface of the polymer electrolyte was absorbed with a filter paper, the membrane was weighed (W_i). The polymer electrolyte was weighed every 10 min at room temperature until the weight did not further change, the weight (W_f) and thickness recorded. In this article, the electrolyte uptake and leakage are calculated by the following equations:

$$\text{Electrolyte uptake} = \frac{W_f - W_0}{W_0}$$

$$\text{Electrolyte leakage} = \frac{W_i - W_f}{W_i - W_0}$$

where W_0 is the weight of polymer membrane, W_i and W_f are the initial and equilibrium weights of the membrane after absorbing the liquid electrolyte, respectively.

2.5. Conductivity measurements

AC impedance and conductance measurements were performed over the frequency range of 1 Hz–1 MHz on an Autolab model Pgstat 30 potentiostat/Galvanostat. A refrigerated circulator temperature controller was used to control the temperature of the measurements. The ionic conductivity of the blend polymer electrolyte (10 mm in diameter and 0.2–0.4 mm thick) was determined by measuring the complex impedance of cells formed by sandwiching the polymer electrolyte sample between two blocking stainless steel electrodes (diameter 10 mm). Conductivity was calculated from the bulk resistance obtained from the impedance spectrum. Samples were equilibrated at the experimental temperature for 30 min before each measurement. The complex impedance spectra were measured from 15 to 90 °C.

2.6. Electrochemical stability

The electrochemical stability of the electrolyte was determined by running linear sweep voltammetry using a two-electrode cell on the Pgstat 30 at room temperature. Both counter electrode and working electrode were Pt coated stainless steel. The lithium ion cell was assembled in a glove box by sandwiching the electrolyte film between the anode and the cathode. The anode and cathode were prepared by coating anode and cathode slurries onto copper and aluminum substrates, respectively. The anode and cathode slurries were obtained by mixing electroactive materials ($LiCoO_2$ for cathode and MCMB for anode) with super-P carbon black, and a binding material in a specific weight ratio.

2.7. Physicochemical studies

Fourier transform infrared (FTIR) spectra were recorded for free standing thin films or films on Si substrates using a Bio-Rad 155 FTIR spectrometer at ambient temperature in the range of 400–4000 cm^{-1} with a wavenumber resolution of 4 cm^{-1}. Scanning electron microscopy (SEM) and energy dispersive spectroscopy (EDS) studies were done with a Hitachi S-800 at 15 kV. X-ray powder diffraction studies were carried out with a Shimadzu XRD-6000 X-ray diffractometer using Cu Kα radiation at 30 kV and 30 mA. Thermogravimetric analysis (TGA) was performed with a Perkin–Elmer TGA-7 thermal analysis system using dry nitrogen (or oxygen) as a carrier gas at a flow rate of 100 ml/s. The TGA experiments were conducted from 25 to 900 °C with a linear heating rate of 10 °C/min. Differential scanning calorimetry (DSC) measurements were performed on a Mettler Toledo DSC 822^e apparatus. Samples were heated from 25 to 80 °C at a heating rate of 10 °C/min. and then cooled to −60 °C. Three heating–cooling cycles were recorded. Melting point (T_m) and melting enthalpy (ΔH_m) were determined from the DSC endothermic peaks on both the first and the second heating runs. Glass transition temperatures (T_g) were estimated as the mean value between onset and endset temperature of the process.

3. Results and discussion

3.1. Morphology of the porous membranes

Fig. 1 shows the typical SEM photographs of PVdF-HFP/5%P123 hybrid porous polymer films obtained from various fabrication conditions. Two distinct morphologies were observed. The cast films showed a porous structure with the pore diameter of 1–5 μm. Films prepared by spin coating showed a denser structure with lower porosity. We found that the porosity of the polymer films also depended on the solvent used. Polymer films prepared from solution with higher acetone (solvent) content had smaller pore sizes and higher pore density. The weight ratio of the electrolyte solution uptake to the polymer substrate will increase as pore volume increased. We expect that the conductivity of polymer films (after soaking in electrolyte solution) prepared by using blade casting method will be higher due to their higher pore density. Therefore, the samples for the following study were made by the blade casting method using NMP:acetone (4.7:3.3) as a solvent.

Fig. 2 shows the SEM microscopic images of the PVdF-HFP/P123 films with various P123 contents. The films cast from the mixture of PVdF-HFP and P123 were opaque and smooth in appearance and did not show any phase separation in the SEM image at the P123 content up to 70 wt%. However, when the ratio of P123 to PVdF-HFP is higher than 50 wt%, the mechanical strength (especially the shearing stress) became poor. The cross section SEM pictures of PVdF-HFP/P123 films cast from NMP:acetone (4.7:3.3) solutions were shown in Fig. 2(b). Polymer films with P123 content less than 70 wt% showed a sponge-like structure. The size of the pores decreased as the content of P123 increased. Nevertheless, rather compact wall with large straight channels was observed in PVdF-HFP/70%P123. The channel-like morphology may be the reason that PVdF-HFP/P123 (70%) has the highest conductivity among the electrolyte membranes we prepared in this study. The conductivity data will be presented later in the article.

3.2. Thermal properties of the porous membranes

The thermal stability of the as-prepared polymer electrolytes was test with thermogravimetric analysis,

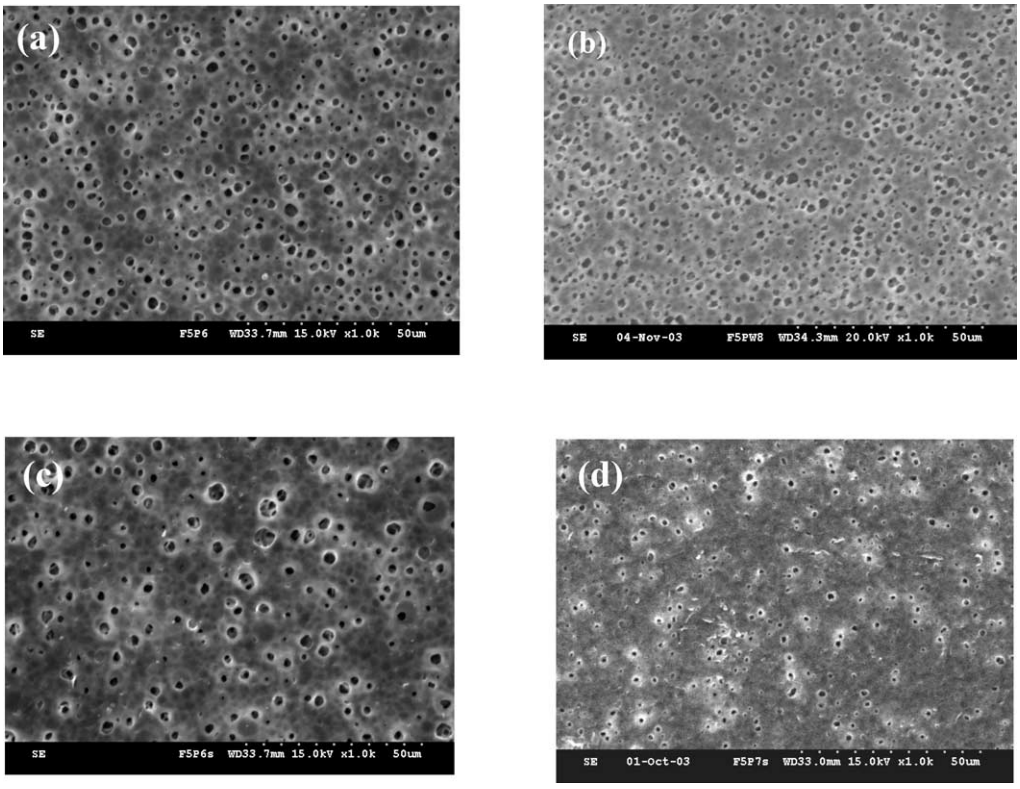

Fig. 1. SEM micrographs of PVdF-HFP/5%P123 (a) blade cast from pure NMP solution; (b) blade cast from NMP: acetone (volume ratio: 4.7:3.3) solution; (c) spin-coated from pure NMP solution; (d) spin-coated from NMP: acetone (volume ratio: 4.7:3.3) solution.

Fig. 3, which showed that the thermal stability of PVdF-HFP was better than that of P123 (Fig. 3(a)). The thermal stability of the blends thus decreased with increasing P123 content. Except PVdF-HFP/70%P123, the hybrid polymers were stable up to 250 °C, high enough to be applied in lithium ion batteries. DSC was used to investigate the compatibility of PVdF-HFP and P123 in PVdF-HFP/P123 blends. A typical DSC curve of PVdF-HFP/30%P123 films is shown in Fig. 4 and the thermal data of all polymer blends are listed in Table 1. The thermogram of PVdF-HFP/P123 films exhibits an endothermic peak, an exothermic peak and one glass transition temperature. Apparently, the melting point and melting enthalpy of first heating-cooling cycle is different from those of second and third cycles (2nd and 3rd cycles are identical). This implies that heat treatment will affect the structure of the polymer hybrid. For compatible polymer blends, the glass-transition temperature (T_g) of the polymer blend is expected to be intermediate between that of the two components. In fact, it is difficult for the T_g of PVdF-HFP/P123 blended film to be detected because PVdF-HFP is semi-crystalline and P123 is amorphous. Nevertheless, the crystallinity depression of PVdF-HFP was observed when P123 was added. The crystallinity of pure PVdF-HFP film was assumed to be 100% and all blended polymer films have crystallinity less than 73% and decreased as the P123 content increased. The drop in crystallinity indicates that P123 is somewhat compatible with PVdF-HFP. Therefore, the depression of the crystalline portion of PVdF-HFP can be used as a criterion for compatibility, and suggests that P123 is compatible with PVdF-HFP.

3.3. Porosity and pore size of PVdF-HFP/P123 membrane

In order to explore the porosity of the polymer membranes, *n*-butanol absorption [27,28] was performed as described in the experimental section. It was found that the porosity of PVdF-HFP/P123 films increased with increasing P123 content up to 50%; although it does not follow a linear relation (Fig. 5). Interestingly, as the content of P123 increased from 50 to 70%, the porosity was significantly decreased. The porosity for PVdF-HFP/70%P123 film was measured to be 0.31%, which is only half time of that of PVdF-HFP/50%P123 film. The electrolyte uptake of PVdF-HFP/70%P123 is also lower than that of PVdF-HFP/50%P123. However, the conductivity of PVdF-HFP/70%P123 after electrolyte uptake is higher than PVdF-HFP/50%P123, probably due to the channel structure of the former (Fig. 2(b)). The detailed studies of the relationship between the pore volume, pore size, and the electrolyte uptake of the polymer membrane as well as the ionic conductivity of the polymer electrolyte will be discussed later in the article.

SEM micrographs displayed only the pores on the surface and *n*-butanol absorption measured only the porosity (or pore volume) of the polymer membranes. In order to

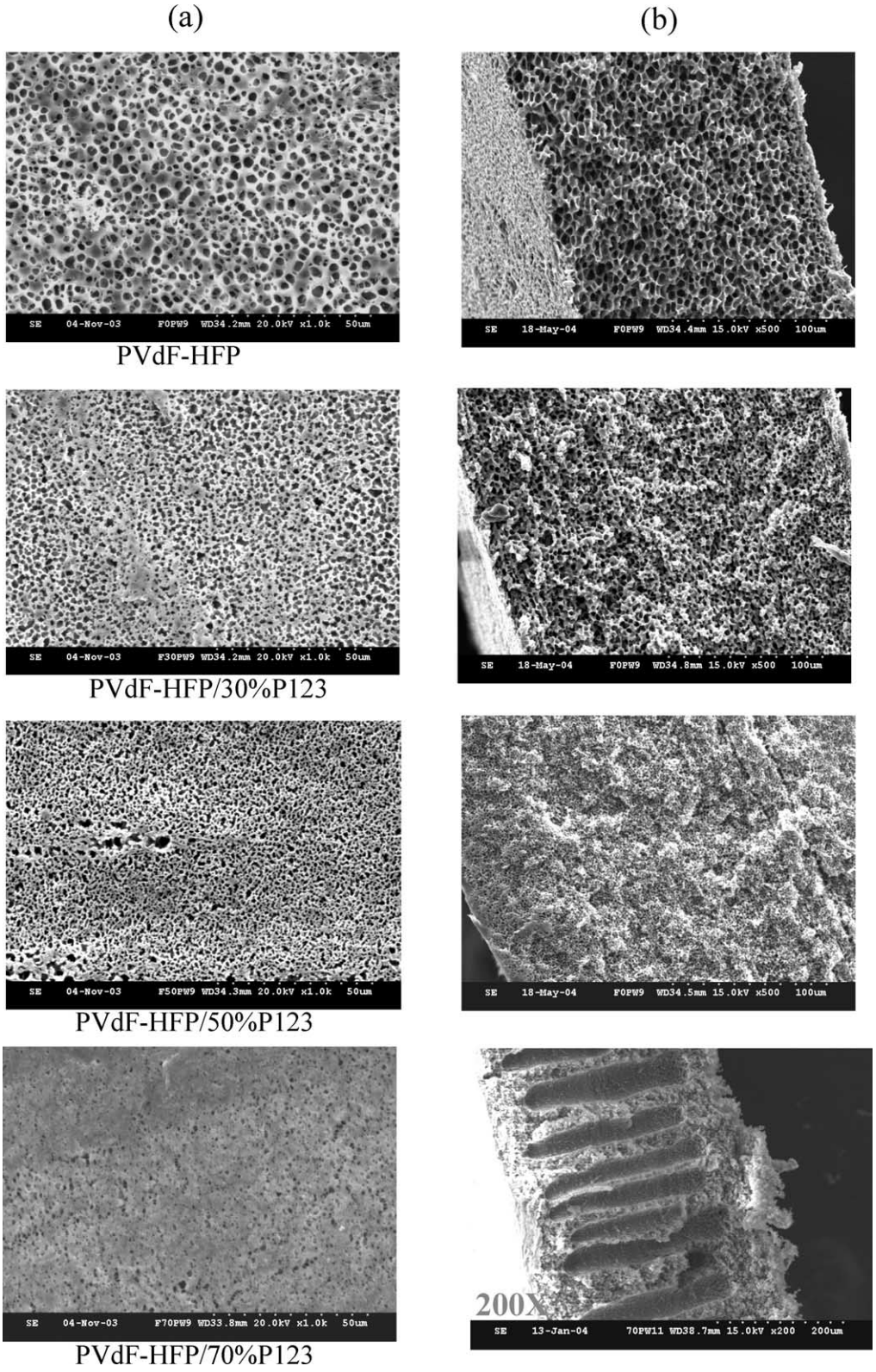

Fig. 2. SEM micrographs of PVdF-HFP with various amounts of P123 (a) top view (the phase toward the Teflon; magnification: 1000) (b) cross-sectioned view (magnification: 500 except that of PVdF-HFP/70%P123).

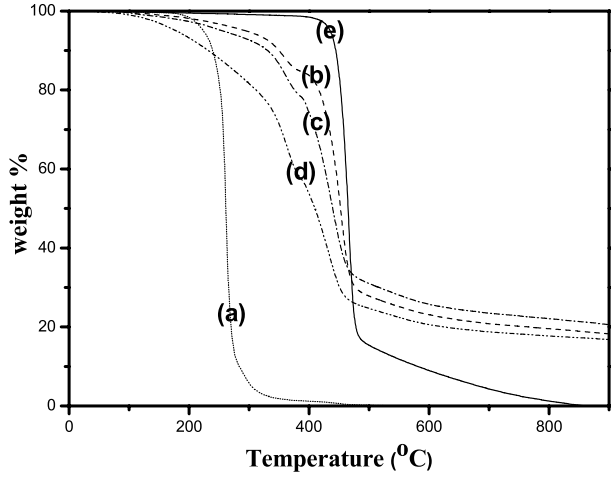

Fig. 3. TGA curves of (a) P123, (b) PVdF-HFP/30%P123, (c) PVdF-HFP/50%P123, (d) PVdF-HFP/70%P123, and (e) PVdF-HFP.

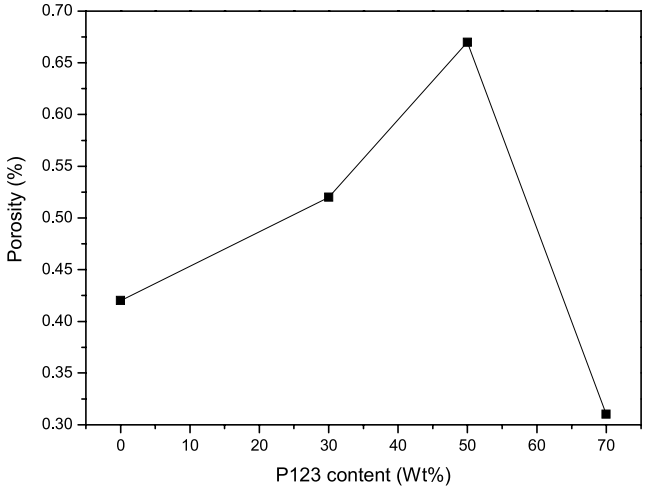

Fig. 5. Porosity vs P123 content of PVdF-HFP/P123 membranes.

explore the pore size (especially nano-sized pores) of the membrane in the bulk, nitrogen adsorption isotherms were measured and the data are listed in Table 2. The nitrogen adsorption isotherm (Fig. 6) showed that the total volume of pores smaller than 300 nm is very small in pure PVdF-HFP and the curve of BJH desorption pore volume (Fig. 7(a)) revealed that pure PVdF-HFP membrane did not have a well-defined pore structure. Nevertheless, when a small amount (5 wt%) of P123 was blended into the polymer, a nitrogen isotherm resembling a Type-II (according to the IUPAC classification [29]) was observed as displayed in Fig. 6. Type-II isotherms have been reported for several as-synthesized surfactant-containing ordered mesoporous materials (OMMs) [30,31]. It has been generally observed in macroporous solids and indicates that there may be a pronounced stage of monolayer formation [32]. However, the pore size distribution calculated from the BJH method [33] (Fig. 7(b)–(d)) showed that some well-defined mesopores with sizes between at 2–15 nm were observed in PVdF-HFP/P123.

It is interesting to know the effect of P123 on the porosity and pore sizes of PVdF-HFP/P123. P123 is a water-soluble block copolymer, which contains two different segments

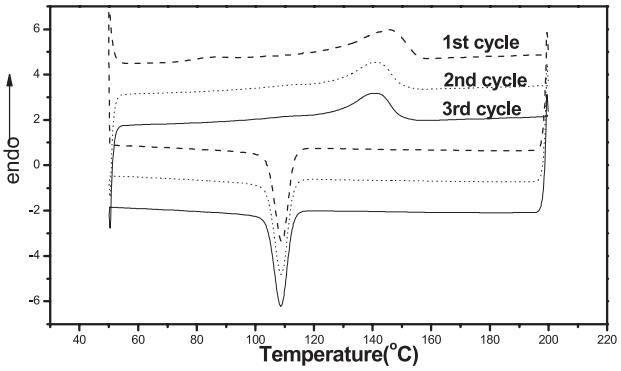

Fig. 4. DSC patterns of PVdF-HFP/30%P123.

with distinct polarity. PVdF-HFP is also a block copolymer containing poly-vinylidene-fluoride and poly-hexafluoro-propylene segments (these two polymer blocks have different polarity). These two block polymers are mixable; therefore no phase separation was found in PVdF-HFP/P123 blends. P123 is more soluble in NMP compared to PVdF-HFP; NMP molecules in PVdF-HFP/P123 blend dispersed more homogenous (i.e. the number of NMP drops increased and the sizes decreased) than that in pure PVdF-HFP. When NMP was extracted by water, smaller pores and higher pore density were formed in polymer membrane. Furthermore, P123 was a water-soluble polymer; some polymer chains may also be extracted by water during the phase inversion process and the amorphous nature of P123 can reduce the shrinkage of the polymer wall when NMP was extracted with water. These two factors may account for increasing in pore volume when P123 was blended into PVdF-HFP.

The formation of well-defined nano-pores in PVdF-HFP/P123 is also a valuable phenomenon to be noted. P123

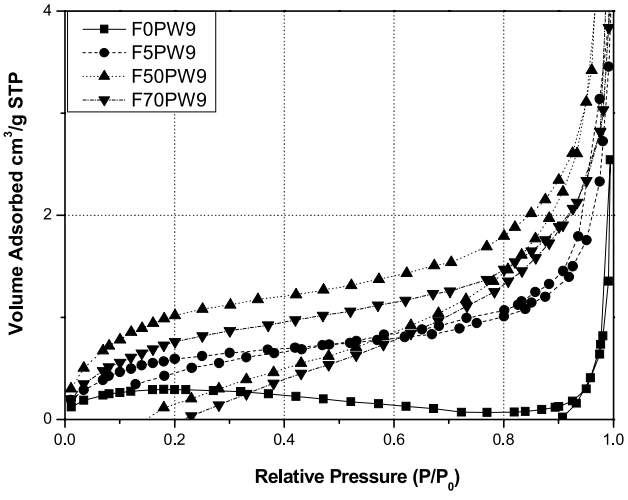

Fig. 6. Nitrogen adsorption isotherms of pure PVdF-HFP and PVdF-HFP/P123.

Table 1
The thermal data of PVdF-HFP/P123 polymer films

Thermal parameter	T_m (°C)			Crystallinity (%)			T_c (°C)			Heat of crystallization (J/g)		
Cycle number	1st	2nd	3rd	1st	2nd	3rd	1st	2nd	3rd	1st	2nd	3rd
PVdF-HFP	143	143	142	100	75	74	108	108	107	−29	−30	−30
PVdF-HFP/30%P123	145	141	141	73	56	56	109	109	109	−24	−24	−24
PVdF-HFP/50t% P123	139	143	143	39	52	53	108	108	108	−23	−23	−23
PVdF-HFP/70t% P123	143	142	142	29	44	44	108	108	108	−19	−19	−19

is known as a polymer surfactant; it forms micelles in water at critical concentration of 4.4×10^{-6} M [34]. It may also form micelles (maybe inverse micelles or bi-layer micelles) in NMP/acetone mixed solvents, although the conformation of P123 in NMP/acetone was unknown in this moment. P123 micelles (maybe inverse micelles or bi-layer micelles) can be also extracted with steam during the phase inversion process, pores with the size similar to that of the micelle were formed. Furthermore, in P123 inverse-micelle, the hydrophilic (EO) head may enclose nano-sized NMP drops and the hydrophobic (PO) tail integrates with PVdF-HFP chains. Therefore, only NMP molecules were replaced with water during the phase inversion process; nano-sized pores were molded. The variation of pore sizes and pore density of PVdF-HFP/P123 membrane with P123 content indicated that the interactions between PVdF-HFP, P123, and NMP are very complicated and the film fabrication processes may have a great effect on the pore formation of polymer membranes. More experiments are underway to solve these puzzles and the results will be reported elsewhere.

In order to check the existence of intermolecular interactions between P123 and PVdF-HFP, FTIR spectra of P123, PVdF-HFP, and PVdF-HFP/P123 membranes with different P123 contents were investigated. The IR patterns of PVdF-HFP/P123 with P123 less than 30% are similar to that of pure PVdF-HFP. Peaks belonging to P123 appeared only when the content of P123 was greater than 50%. The peak at 1107 cm^{-1} corresponding to absorption for the C–O stretching of pristine P123 was shifted to lower frequency by 5–10 cm^{-1} for the PVdF-HFP/P123 membranes as shown in Fig. 8. This observation can be interpreted [35] in terms of the specific interaction between the fluorine in PVdF-HFP and the carbon connected to oxygen of P123.

Table 2
The surface area and pore volume of PVdF-HFP/P123 obtained from nitrogen adsorption isotherm

Sample	Adsorption data	
	Surface area (m^2/g)	Pore volume (cm^3/g)
PVdF-HFP	1.0214	3.93×10^{-3}
PVdF-HFP/5%123	2.0527	6.21×10^{-3}
PVdF-HFP/50%P123	4.0811	17.2×10^{-3}
PVdF-HFP/70%P123	3.1503	8.04×10^{-3}

The fluorine in PVdF-HFP and the carbon in P123 conduct as a Lewis base and a Lewis acid, respectively. The electron donating of fluorine to carbon weakens the C–O bond, and the absorption for C–O stretching shifts to lower wavenumber.

3.4. Electrolyte uptake, solvent leakage, and ionic conductivity of polymer membranes and electrolytes

Table 3 lists the pore volume, electrolyte uptake, and room temperature conductivity of PVdF-HFP/P123 electrolytes with various P123 concentrations. It was found that the pore volume increased as the weight of P123 increased up to 50 wt% and then decreased significantly (the pore volume of PVdF-HFP/70%P123 was even smaller than that of pure PVdF-HFP). As a consequence, the electrolyte uptake also increased and then decreased as the weight of P123 increased. Nevertheless, the electrolyte uptake of PVdF-HFP/70%P123 is much higher than that of pure PVdF-HFP although the latter has higher pore volume. This result suggests that blending P123 into PVdF-HFP can enhance the electrolyte absorption, due to the higher affinity of P123 toward EC/PC molecules (the solvents of the electrolyte). The affinity between P123 and electrolyte was also illustrated based on solvent leakage of PVdF-HFP/P123, as shown in Fig. 9. It was found that the solvent leakage was reduced substantially when small amounts of P123 were added. The modification of the pore size and increasing of the attraction of the polymer membrane to the electrolyte helps electrolyte uptake and avoids solvent leakage, factors that will enhance the performance of the polymer electrolyte.

Variable temperature conductivity of PVdF-HFP/P123 is displayed in Fig. 10. The conductivity increased with increasing temperature, a typical behavior of lithium polymer electrolytes. Similar behavior has also been observed in PEO-based electrolytes. The room temperature conductivity of PVdF-HFP/P123 with P123 concentrations greater than 30 wt% was $>1\times10^{-3}$ S/cm, high enough for practical applications in lithium ion batteries. Furthermore, the conductivity of both PVdF-HFP/50%P123 and PVdF-HFP/70%P123 was higher than 1×10^{-3} S/cm at

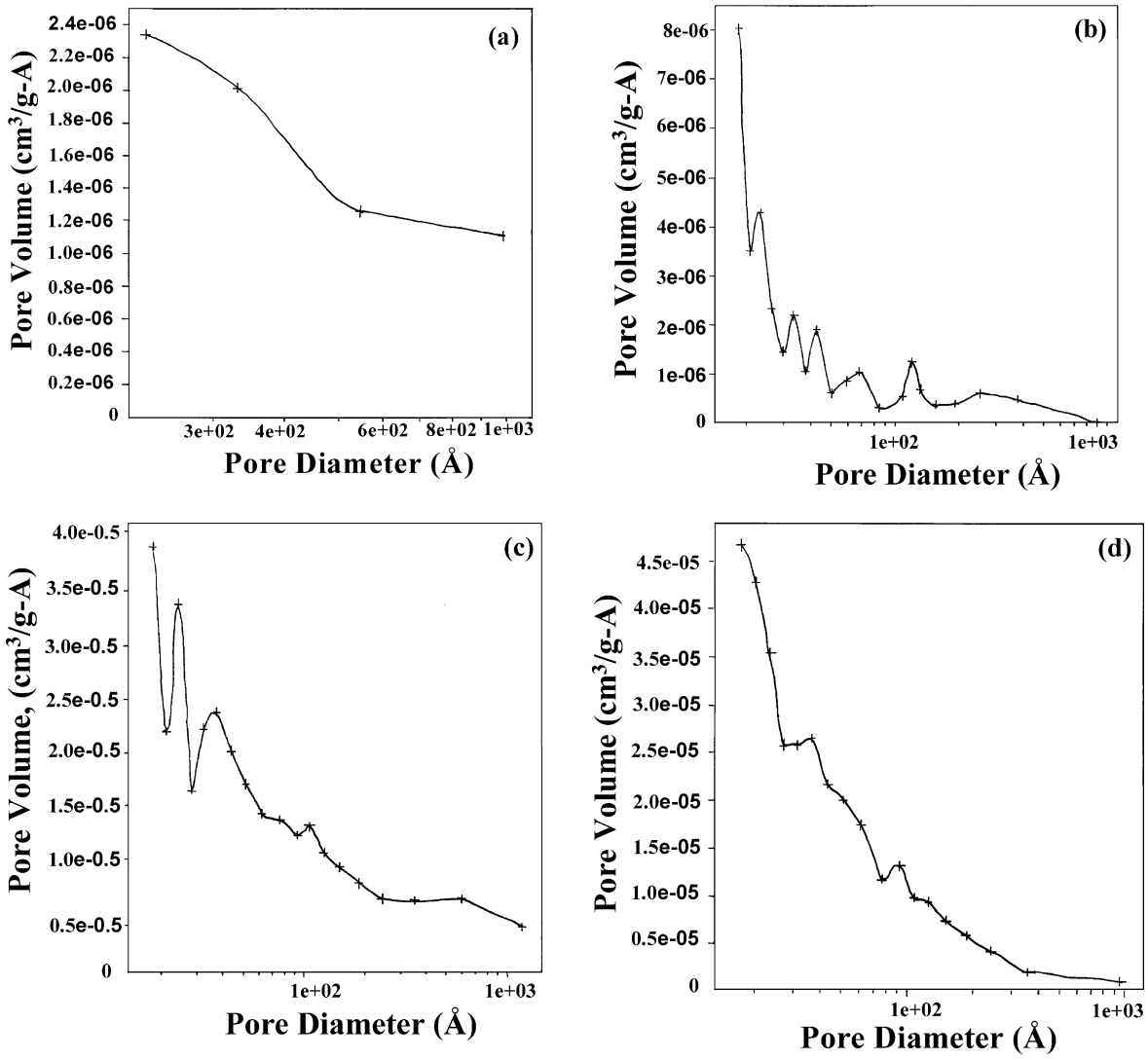

Fig. 7. BJH desorption curves of (a) PVdF-HFP, (b) PVdF-HFP/5%P123, (c) PVdF-HFP/50%P123, and (d) PVdF-HFP/70%P123.

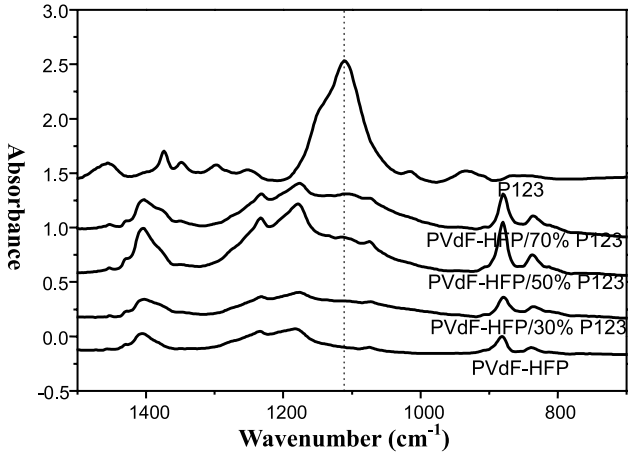

Fig. 8. IR spectra of PVdF-HFP and PVdF-HFP/P123 membranes.

Table 3
The pore volume, room temperature conductivity and electrolyte uptake of the polymer films with various P123 content

Sample	Property		
	Pore volume[a] (cm^3/g)	Electrolyte uptake (wt%)	Room temperature conductivity (S/cm)
PVdF-HFP	0.40	59.1	4.9×10^{-4}
PVdF-HFP/5% P123	0.57	62.6	4.2×10^{-4}
PVdF-HFP/ 10% P123	0.76	71.8	4.6×10^{-4}
PVdF-HFP/ 15% P123	0.75	102	5.9×10^{-4}
PVdF-HFP/ 30% P123	0.88	130.5	1.3×10^{-3}
PVdF-HFP/ 50% P123	1.17	224.0	2.0×10^{-3}
PVdF-HFP/ 70% P123	0.25	120.6	2.6×10^{-3}

[a] Pore volume calculated from *n*-butanol absorption.

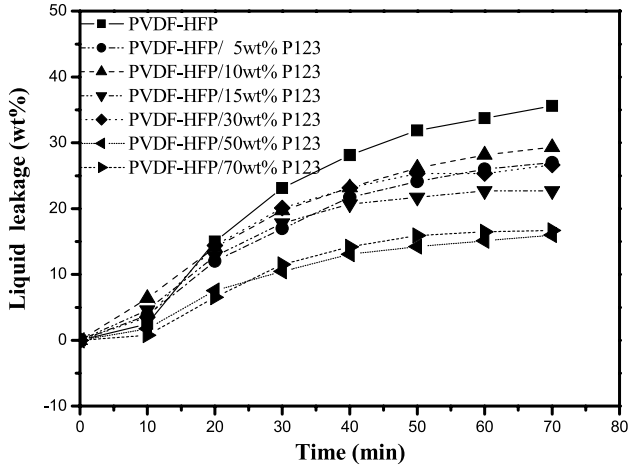

Fig. 9. Solution leakage of PVdF-HFP and PVdF-HFP/P123 electrolytes in an open container in a dry box.

temperatures as low as 10 °C (the lowest temperature we can measure in our system).

3.5. Electrochemical stability

For determining the electrochemical stability window of the blended polymer electrolyte, a linear sweep voltammetry experiment was performed in the potential range of 0.0–6.0 V (vs Li/Li^+) with a scan rate of 5 mV/S. Fig. 11 shows the current–voltage response of a Pt coated stainless steel electrode/polymer electrolyte/Pt cell. The onset current flow is associated with the decomposition voltage of the electrolyte. It was found that the current flow is very small when the voltage is below 4.5 V (vs Li/Li^+) except in PVdF-HFP/70%P123 which has a small current at potentials less than 4.5 V. The fact that the oxidation occurs at potentials higher than 4.5 V for all PVdF-HFP/P123 with P123 concentrations less than 70 wt% makes these materials very suitable for Li^+ battery applications.

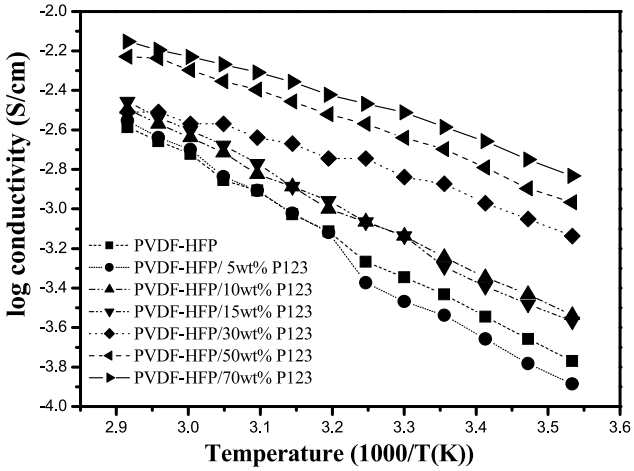

Fig. 10. Variable temperature conductivity of PVdF-HFP and PVdF-HFP/P123 polymer electrolytes.

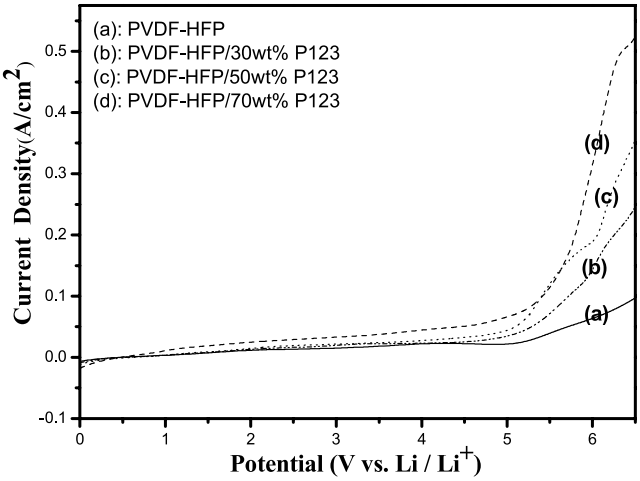

Fig. 11. Linear sweep voltagramms of PVdF-HFP and PVdF-HFP/P123 electrolytes.

To evaluate the electrochemical performance of a lithium ion polymer cell using PVdF-HFP/P123 electrolytes, MCMB/PVdF-HFP/P123 polymer electrolyte/$LiCoO_2$ cells were constructed. The assembled cells were subjected to preconditioning with a cut-off voltage of 4.2 V for the upper limit and 3.0 V for the lower limit at a charge rate of 150 μA/cm^2. Fig. 12 shows the performance of the lithium ion polymer cell. It can light-up a small electric bulb at the effective electrode surface as small as 0.38 cm^2. Detailed studies of the electrochemical performance of the lithium ion cell using PVdF-HFP/P123 polymer electrolyte are in progress.

4. Conclusion

PVdF-HFP/P123 polymer membranes with mesoporous structures were fabricated by mixing PVdF-HFP and

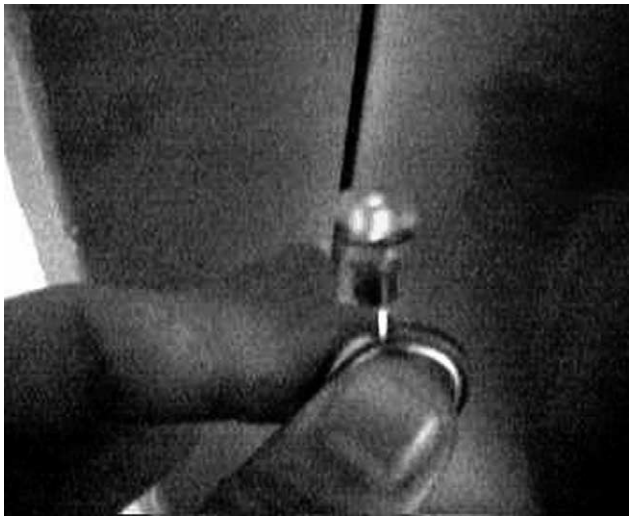

Fig. 12. The performance of a MCMB/PVdF-HFP/P123/$LiClO_4$/$LiCoO_2$ cell.

surfactant polymer, P123. The porosity of the PVdF-HFP/P123 membranes increased with increasing concentration of P123 up to 50 wt%. A significant amount of mesopores were formed at P123 contents of 5–30 wt%. This may be due to the formation of P123 micelles. The ability to make polymer membranes with smaller pore sizes and high pore density was attributed to the more pronounced phase separation between NMP and polymer in PVDF-HFP/P123. The increase of the porosity significantly increases the ionic conductivity of the polymer membranes after electrolyte uptake. The affinity between the P123 and the electrolyte solution also reduced the electrolyte leakage, thus enhanced the performance of the polymer electrolyte. This is the first report in which blending a polymer surfactant in PVdF-HFP was shown to form nano-sized pores, which may have an impact on the design of porous polymer electrolytes for lithium ion batteries.

Acknowledgements

We gratefully acknowledge the Chung-Shan Institute of Science and Technology and the National Science Foundation of the Republic of China for the financial support of this work.

References

[1] Vincent CA, Scrosati B. Modern batteries. An introduction to electrochemical power sources. 2nd ed. London: Arnold; 1997.
[2] Scrosati B. Nature 1995;373:557.
[3] Gray FM. Solid polymer electrolyte—fundamentals and technological applications. New York: VCH; 1991.
[4] Fenton DE, Perker JK, Wright PV. Polymer 1973;14:589.
[5] Michot T, Nishimoto A, Watanabe M. Electrochim Acta 2000;45: 1347.
[6] Boudin F, Andrieu X, Jehoulet C, Olsen II. J Power Sources 1999; 81/82:804.
[7] Michot T, Nishimoto A, Watanabe M. Electrochim Acta 2000;45: 1347.
[8] Bohnke O, Frand G, Rezrazzi M, Rousselot C, Truche C. Solid State Ionics 1993;66:97.
[9] Bohnke O, Frand G, Rezrazzi M, Rousselot C, Truche C. Solid State Ionics 1993;66:105.
[10] Appetecchi GB, Croce F, Scrosati B. Electrochim Acta 1995;40:99.
[11] Abraham KM, Alamgir M. J Electrochem Soc 1990;137:1657.
[12] Watanabe M, Kanba M, Nagaoka K, Shinchara I. J Polym Sci, Polym Phys Ed 1983;21:939.
[13] Sukeshini AM, Nishimoto A, Watanabe M. Solid State Ionics 1996; 86–88:385.
[14] Appetecchi GB, Dautzenberg G, Scrosati B. J Electrochem Soc 1996; 143:6.
[15] Appetecchi GB, Croce F, Scrosati B. J Power Sources 1997;66:77.
[16] Kim HT, Kim KB, Kim SW, Park JK. Electrochim Acta 2000;45: 4001.
[17] Rhoo HJ, Kim HT, Park JK, Hwang TS. Electrochim Acta 1997;42: 1571.
[18] Wang H, Keyha JB, Yarovoy YK, Wunder SL. Mater Res Soc Symp Proc 1999;548:347.
[19] Boudin F, Andriew X, Jehoule C, Olsen II. J Power Sources 1999; 81/82:804.
[20] Kim DW, Sun YK. J Power Sources 2001;102:41.
[21] Oh B, Kim YR. Solid State Ionics 1999;124:83.
[22] Huang H, Wunder SL. J Electrochem Soc 2001;148:A279.
[23] Huang H, Wunder SL. J Power Sources 2000;97:4001.
[24] Huang H, Wunder SL. J Power Sources 2001;98:649.
[25] Saito Y, Stephan AM, Kataoka H. Solid State Ionics 2003;160:149.
[26] Lightfood PM, Metha A, Bruce PG. Science 1993;262:883.
[27] Chi SK, Seung MOh. Electrochim Acta 2001;46:1323.
[28] Kim KM, Park N-G, Ryu KS, Chang SH. Polymer 2002;43:3951.
[29] Sing KSW, Everett DH, Haul RAW, Moscou L, Pierotti RA, Rouquerol J, et al. Pure Appl Chem 1985;57:603.
[30] Kruk M, Jaroniec M, Ryoo R, Joo SH. Chem Mater 2000;12:1414.
[31] Park M, Komarneni S. Microporous Mesoporous Mater 1998;25:75.
[32] Kruk M, Jaroniec M. Chem Mater 2001;13:3169.
[33] Barrett EP, Joyner LG, Halenda PP. J Am Chem Soc 1951;73:373.
[34] Kozlov MY, Melik-Nubarov NS, Batrakova EV, Kabanov AV. Macromolecules 2000;33:3305.
[35] Song JM, Kang HR, Kim SW, Lee WM, Kim HT. Electrochim Acta 2003;48:1339.